JOURNAL OF MATERIALS SCIENCE **40** (2005) 4307–4312

Study of friction stir welded A319 and A413 aluminum casting alloys

N. A. RODRIGUEZ, E. ALMANZA, C. J. ALVAREZ
Departamento de Metal-Mecánica, Instituto Tecnológico de Saltillo, Venustiano Carranza 2400, Saltillo, Coahuila 25280 Mexico

L. E. MURR
Department of Metallurgical and Materials Engineering, University of Texas at El Paso, El Paso, TX 79968 USA

Cast aluminum alloys A319 and A413 were friction stir welded using a rotating steel screw tool. The cast microstructures were characterized by numerous inclusions or second phase particles which were homogeneously stirred into the weld zone. TEM analysis illustrated the dynamic recrystallization which facilitates the solid-state flow, and digital microhardness measurements through the base metals and the weld zones illustrate the absence of any property degradation. In fact the comminution of particles in the weld zone decreased the interparticle spacing and increased the corresponding hardness by 15%.

1. Introduction

Friction-stir welding (FSW) is a solid-state technique well suited for joining specially wrought aluminum alloys. The major characteristic of the process is that a rotary tool generates adiabatic heat into the work pieces, and induces plastic deformation and dynamic recrystallization (DRX) of the material.

As a solid-state process, FSW allows the joining of materials that are difficult or impossible to join by conventional processes of welding such as 2xxx and 7xxx series aluminum alloys [1–3]. The work pieces are held on a support base [4]. As illustrated in Fig. 1, FSW involves the advance of a rotary steel screw (pin tool) within a chuck or holder to create a plastic zone which flows around the side to form a weld in the solid state. There is no melting and when the rotational speed (R) and traverse speed (T) of the pin tool are properly adjusted, there is no porosity in the weld zone [4, 5].

Microstructural changes during FSW have been the focus of numerous research papers published recently, especially involving aluminum alloys [1–3, 6–8]. Valerio-Flores *et al*. [9] have demonstrated that microdendritic, second-phase particles formed during aluminum 1100 casting were transported in bulk into the weld zone during FSW as a consequence of the DRX process. More recently, Shindo *et al*. [10] and Fernandez and Murr [11] have also shown that relatively large ($\sim$4 μm mean diameter) SiC dispersed particles in a cast aluminum 359 matrix were also transported in the solid-state into the weld zone during FSW as a consequence of the DRX process which facilitates solid-state flow during FSW.

In the present study, the FSW of two commercial cast aluminum alloys (A319 and A413) was examined. Particular interest focused on the observation of the fate and transport of an array of precipitates and large second-phase particles which are common in these alloys, and which pose particular problems during conventional (thermal) welding by forming porosities and other weak zones in the weld zone.

2. Experimentation

In this study, A319 and A413 aluminum casting alloy plates of 0.6 cm-thickness were friction stir welded, using a rotational speed of 1000 rpm (counter clockwise) and a traverse speed of 2 mm/sec (Fig. 1). The screw or non-consumable pin tool consisted of a steel O-1 tool of 0.6 cm-diameter inserted into a chuck. The composition of each of the alloys is shown in Table I.

Three different weld systems were examined: A319 Al/A319 Al, A413 Al/A413 Al, and A319 AlA413 Al. Sections were cut from the weld face (Fig. 1) and polished in a series of stages. First, the sectioned samples were ground and polished using SiC papers (grit size 80, 220, 320, 400, 600, 800) with water as a lubricant. These samples then were polished with colloidal silica (0.2 μm). The polished samples were etched using a Keller's reagent (150 mL H_2O, 3 mL HNO_3, 6 mL HCl, 6 mL HF). This solution was used at a temperature of 0°C for 20–30 sec. The macrostructures of the weld zone and each base metal were characterized by optical microscopy (OM) (Olympus AH3-UMA) and scanning electron microscopy (SEM) (Phillips Quanta 200). The identification of precipitates or second phase particles was performed by energy dispersive X-ray spectrometry (EDS). A Hitachi H-8000 analytical transmission electron microscope (TEM), operated at 200 kV, and employing a goniometer-tilt stage, was utilized to examine the microstructural evolution of samples.

TABLE I Chemical composition A319 and A413 aluminum alloys (wt%)

Element	%Al	%Si	%Cu	%Fe	%Mn	%Mg	%Zn	%Others
A319	84.85	6.80	3.50	1.20	0.50	0.43	2.40	0.32
A413	86.95	11.16	0.37	0.70	0.17	0.09	0.40	0.16

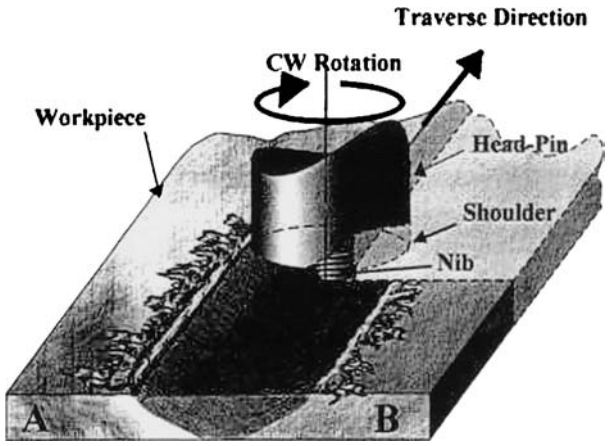

Figure 1 Schematic illustration of the friction stir welding process.

(a)

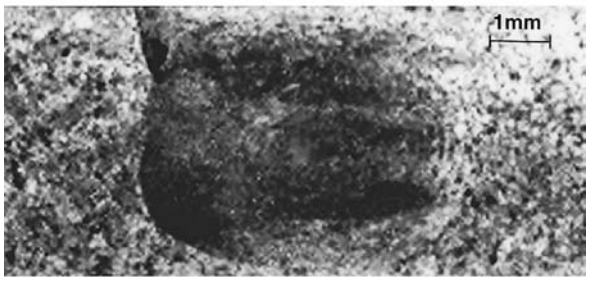

(b)

(c)

Figure 2 Weld zones of (a) nugget A319-A319; (b) nugget A413-A413; (c) nugget A319-A413.

In order to obtain more data about the mechanical properties of the weld and the consistency of the weld compared with the base metal, a Buehler LTD microhardness tester was used (using 100 gf load for 10 sec.) through the thickness sections of the samples. The distance between each hardness indentation was 2 mm. The microhardness profiles were done throughout half of the sections, through the weld zone, and extended from the center of the weld zone towards both sides of the base metal until the value of hardness of the base metal was obtained. The initial hardness values of A319 and A413 plates were 98 HV and 62 HV, respectively.

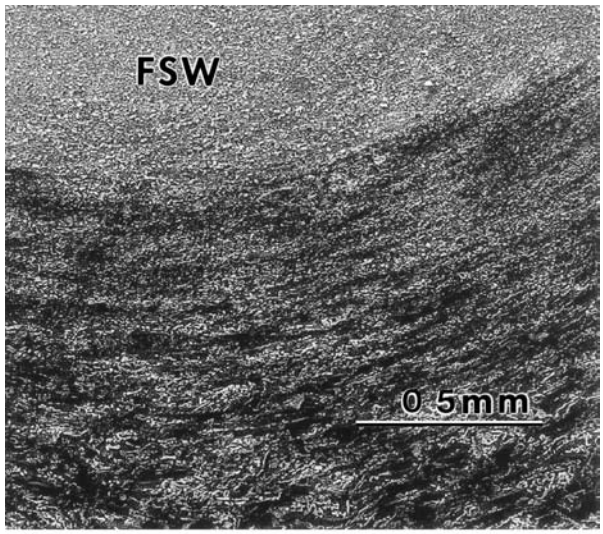

(a)

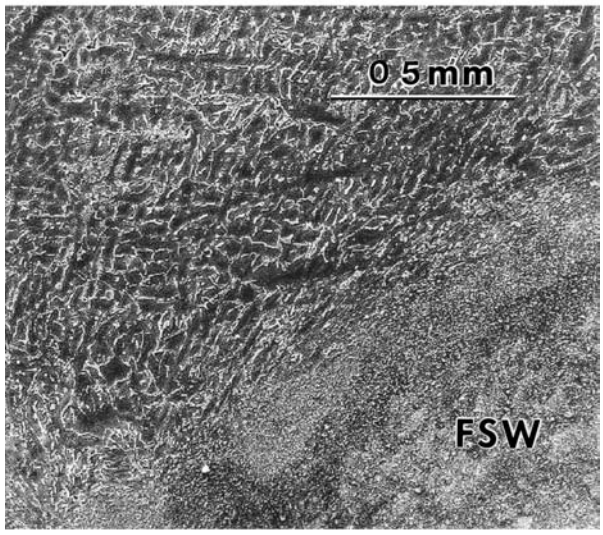

(b)

Figure 3 Magnified views of FSW transition zones in the A413 and A319 aluminum alloys. (a) SEM microstructure of FSW zone and base metal for A413; (b) SEM microstructure of FSW zone and the base metal for A319.

3. Results and discussion

Fig. 2 shows cross-sectional views of the welds for the 3 different systems examined, (1000 rpm and 2 mm/sec). The weld zones have approximately the same width as the diameter of the rotatory tool; 0.6 cm. The microstructures show some degree of continuity due to flow of metal around the rotary tool.

As shown in Figs 3a and b, the FSW zone, especially corresponding to the leading edge or right side of the weld in Fig. 1, is frequently separated by a sharp interfacial area from the unaffected work piece, indicating that the severe deformation associated with the FSW process is accommodated over a very short range, and we observe that the microstructure inside the weld zone is dominated by fine particles which are accentuated by the etchant.

Fig. 4 compares the base microstructure and the FSW zones for the A413 and A319 systems, with the etchant high-lighting the precipitates and inclusions which are characteristic of these cast alloys. The corresponding EDS spectra, which are the basis for their identification [9], are illustrated for comparison in Fig. 5 which also shows the corresponding weld zone microstructures for comparison with the base metal microstructures shown in Fig. 4. The interesting feature illustrated in comparing the base metal and FSW microstructures (Figs 4 and 5) is the breakup and/or redistribution of the initial, base metal phase inclusions in the weld zone. The A319 alloy exhibits a microdendritic cell structure which is completely altered in the re-mixed FSW zone in Fig. 4a and b while the A413 alloy exhibits plates and needles which are largely broken and redistributed in the FSW zone in Fig. 4c and d. The inclusions have higher melting points than the maximum FSW temperatures and there is no reprecipitation or re-solution; consequently no aging or re-aging phenomena.

Since the etchants were more specific to the various inclusion microstructures, the corresponding grain structures were only amenable through TEM analysis as shown typically in Fig. 6 which compares the A413 base grain structure with the A413 FSW zone grain structure. While the A413 base grain size of $\sim$6 μm is only reduced by roughly half in the corresponding FSW zone, there appears to be no noticeable change in the dislocation density; and similar observations also characterized the A319 alloy.

Fig. 7 compares the corresponding microhardness profiles through the weld centers for the A319 an A413 FSW systems where the A319 FSW zone is observed to be roughly 15% harder than the corresponding base metal. The A413 system, by contrast, exhibits a nearly constant hardness from the base metal through the FSW zone. This behavior has been observed for other cast aluminum alloy systems where initial precipitates or inclusions are stirred and re-distributed into the FSW zone [9–11, 13].

It is interesting to note that the hardness increase in the FSW zone observed in the A319 alloy system is due to a noticeably finer inclusion microstructure, i.e. a considerably closer spacing between inclusions than in the A413 system (compare Fig. 4b and d). This hardness increment is vested in a relationship of the form

$$H = H_o + (K/\sqrt{D} + K'\sqrt{\rho}) + K''/\Delta \qquad (1)$$

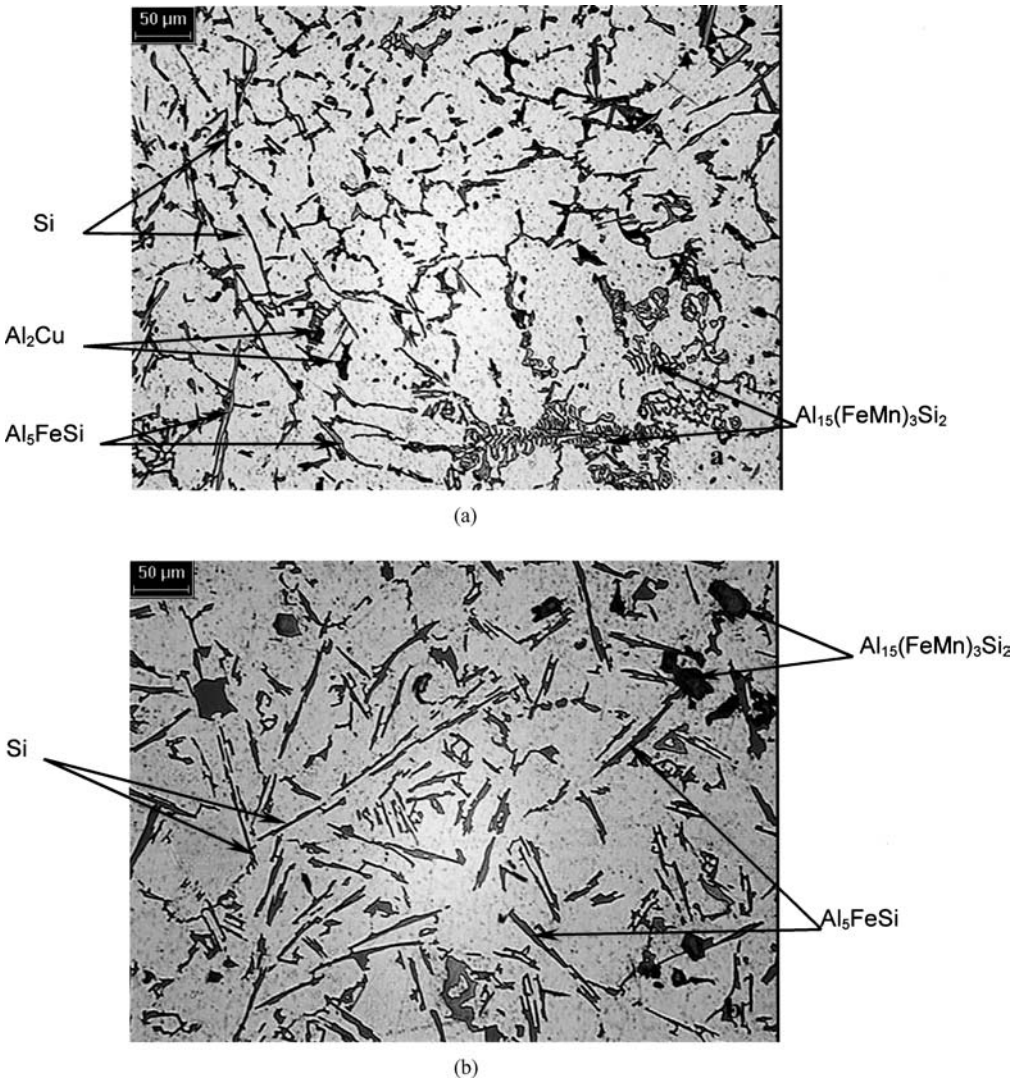

Figure 4 Optical micrographs showing the intermetallic phases in (a) A319 base metal; (b) A413 base metal.

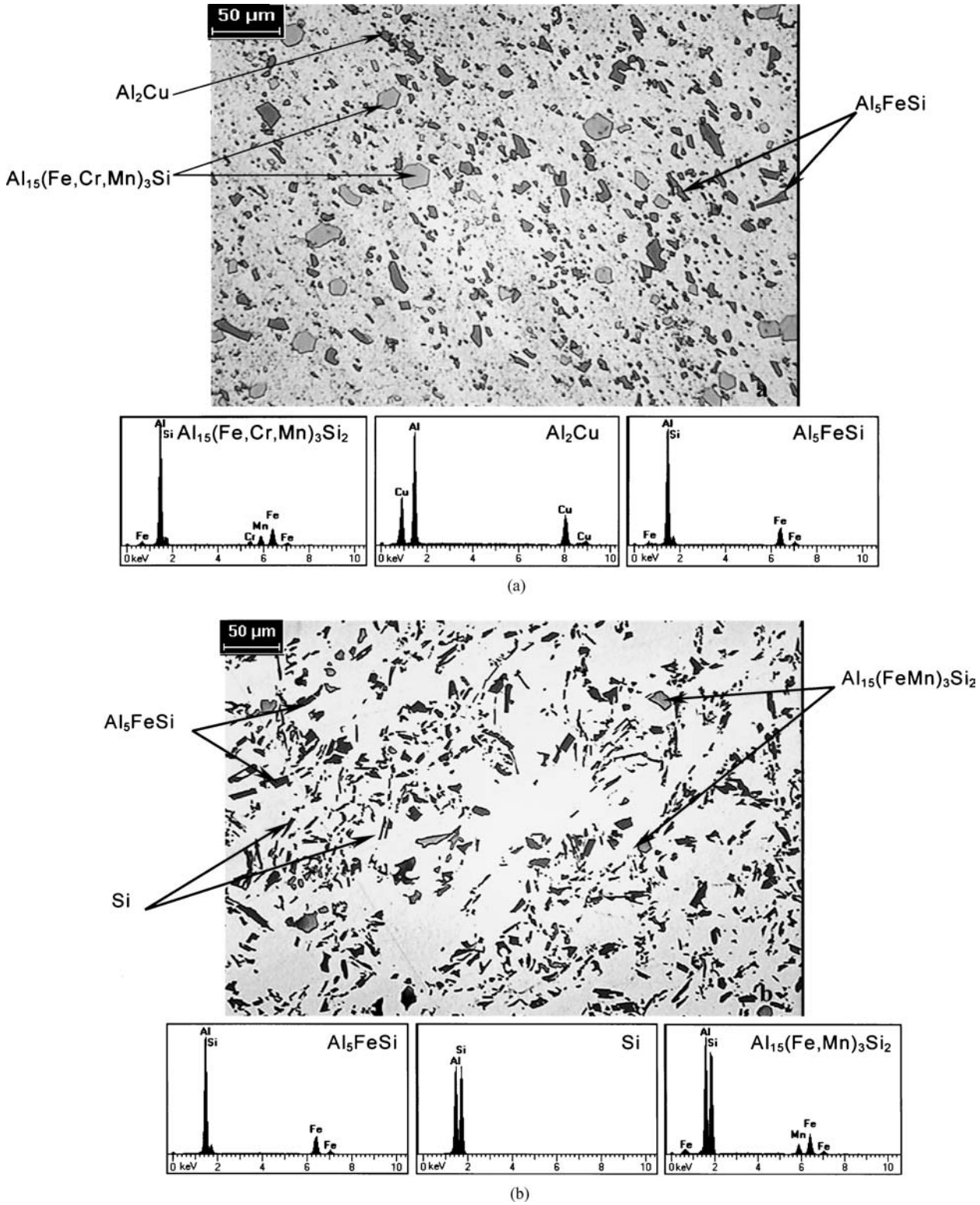

Figure 5 Optical micrographs showing the intermetallic phases in the FSW systems along with corresponding, reference EDS spectra. (a) A319-A319; (b) A413-413.

where H_o and the K values are essentially constant, D is the grain size, ρ is the dislocation density, and Δ is the interparticle spacing or average distance between inclusions; a factor of 5 smaller in Fig. 4b in contrast with Fig. 4d. Equation 1 derives from the fact that in common fcc materials the residual hardness is related to the yield stress (σ_γ) by $H \cong 3\sigma_\gamma$, and the yield stress is represented by a modified Hall-Petch relationship [14], which includes the specific strengthening components D, ρ and Δ essentially as represented in Equation 1 [15]. Since the grain size and dislocation density only change by a small amount, the K''/Δ term in Equation 1 dominates for the A319 alloy, raising the FSW zone hardness. This feature (the increased FSW zone hardness for the A319 alloy) was confirmed by macrohardness measurements using a Rockwell tester, and a correspondingly larger indenter as well.

The 15% hardness increase in the weld zone for the A319 alloy system, while not specifically important from a strengthening perspective, confirms the integrity

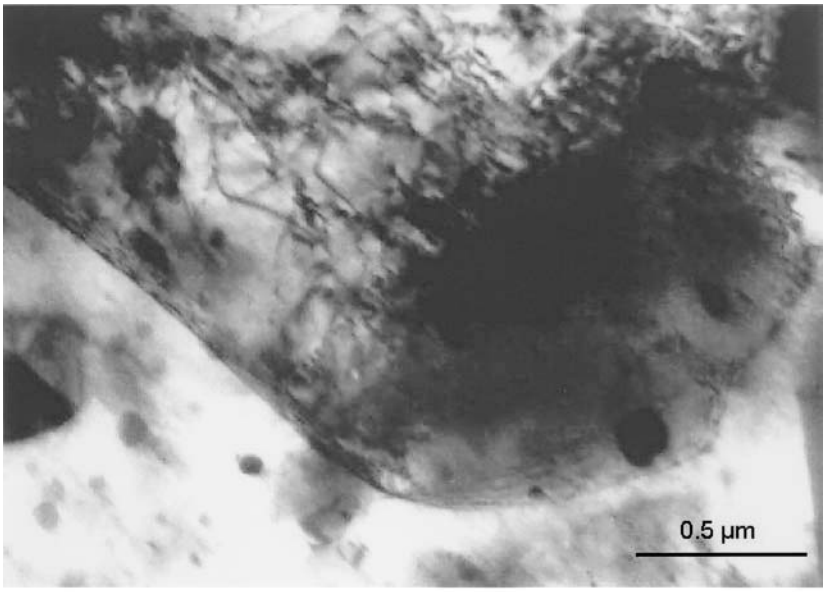

(a)

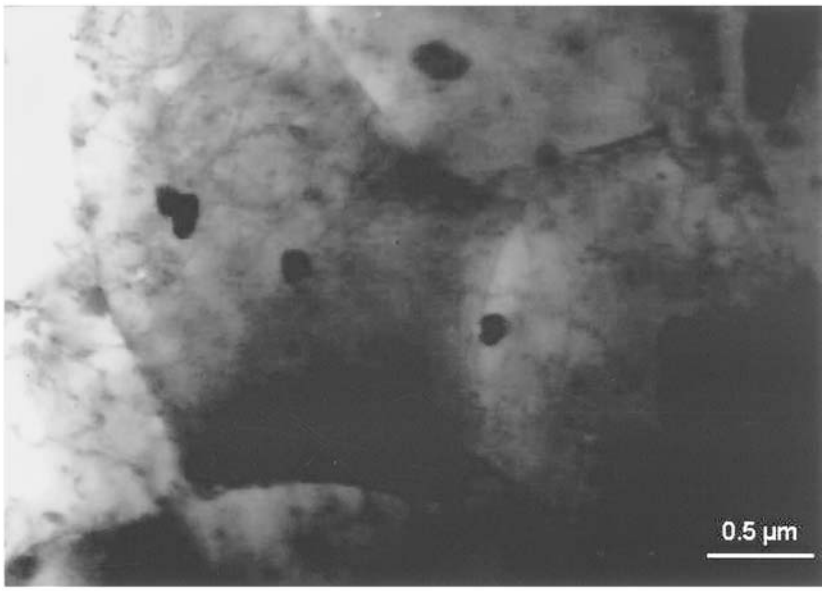

(b)

Figure 6 TEM micrographs (bright-field). (a) A413 base metal; (b) A413 weld zone.

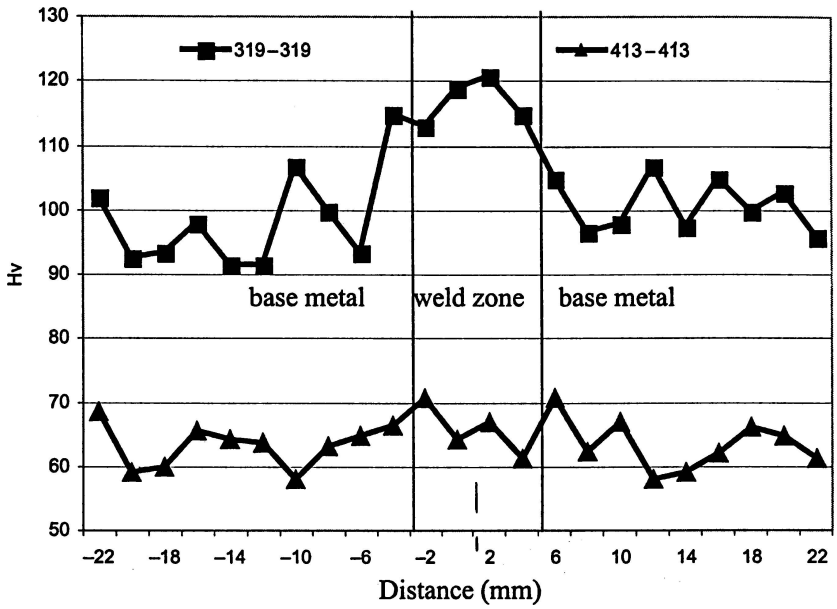

Figure 7 Hardness profile across the weld zone and base metal for the different systems.

of the weld itself, which is in contrast to conventional welding of these types of cast alloys where inclusions create porosities or local cracking which decreases the weld integrity and the weld strength.

4. Conclusions

The FSW of cast aluminum alloys—especially A319 and A413 alloys described herein—is an efficient joining technology which affords no apparent weld zone degradation. Cast metal inclusions and related microstructures are re-distributed within the weld zone by dynamic recrystallization-induced flow in agreement with prior studies on similar FSW systems [9–11].

Acknowledgments

This research was supported by the Consejo del Sistema Nacional de Educación Technológica (Cosnet), Project 442.02-P. The authors thank the Department of Metal-Mecánica of the Instituto Tecnológico de Saltillo as well as the Department of Metallurgical and Materials Engineering of the University of Texas at El Paso, El Paso Texas, for their support in the experimental development of this research.

References

1. H. S. KAZI. and L. E. MURR, Complex flow phenomena associated with friction-stir welding of aluminum alloys, in Friction Stir Welding and Processing, edited by K. V. Jata, M. W. Mahoney, R. S. Mishra, S. L. Semiahin and D. F. Field, (TMS, Warrendale, PA, 2001) p. 139.
2. L. E. MURR, R. D. FLORES, O. V. FLORES, J. C. MC CLURE, G. LIU and D. BROWN, *Mat. Res. Innovat.* **1** (1998) 211.
3. L. E. MURR, YING LI, R. D. FLORES, ELIZABETH A. TRILLO and J. C. MC CLURE, *ibid.* **2**(3) (1998) 150.
4. DAVE. E. NICHOLAS and STEPHAN W. KALLEE, IIW Asian Pacific International Congress Sydney, 29 October to 2 November 2000, in Conjunction with the 12th International Federation of Heat Treatment and Surface Engineering Congress, The New Zealand Institute of Welding 2000 Annual Conference and the WTIA 48th Annual Conference.
5. L. E. MURR, G. SHARMA, F. CONTRERAS, M. GUERRA, S. H. KAZI, M. SIDDIQUE, R. D. FLORES, D. J. SHINDO, K. F. SOTO, E. A. TRILLO, C. SCHMIDT and J. C. MC CLURE, Joining dissimilar aluminum alloys and other metals and alloys by friction stir welding, in Aluminum 2001, edited by S. K. Das, J. G. Kaufman and T. J. Lienert, TMS, (Warrendale, PA, 2001), p. 197.
6. K. V. JATA and S. L. SEMIATIN, *Scripta Mater.* **43** (2000) 743.
7. C. G. RHODES, M. W. MAHONEY, W. H. BINGEL, R. A. SPURLING and C. C. BAMPTON, *ibid.* **36** (1997) 69.
8. YUTAKA S. SATO, IHROYUKI KOKAWA, MASATOSHI ENOMOTO and SHIGETOSHI JOGAN, *Metall. Mater. Trans. A* **30A** (1999) 2429.
9. O. VALERIO-FLORES, L. E. MURR, C. KENNEDY, D. BROWN, S. PAPPU, B. M. NOWAK and J. C. MC CLURE, *Scripta Met.* **38**(5) (1998) 703.
10. D. J. SHINDO, A. R. RIVERA and L. E. MURR, *J. Mater. Sci.* **37** (2002) 4999.
11. G. J. FERNANDEZ and L. E. MURR, *Mater. Character.* **52** (2004) 65.
12. "Solidification Characteristics of Aluminum Alloys," American Foundrymen's Society, Inc., Vol. 3: Dendrite Coherency, 1996.
13. L. E. MURR, Y. LI, E. A. TRILLO, B. M. NOWAK and J. C. MC CLURE, *Aluminum Trans.* **1**(1) (1999) 141.
14. M. A. MEYERS and K. K. CHAWLA, "Mechanical Metallurgy," (Prentice-Hall, Inc., Englewood Cliffs, N.J., 1984).
15. M. A. MEYERS and K. K. CHAWLA, "Mechanical Behavior of Materials," (Prentice-Hall, Upper Saddle River, NJ., 1999, p. 277).

Received 29 June 2004
and accepted 13 April 2005